crystals

MDPI

Article

Effect of Noncovalent Dispersion of Poly(Ethylene Oxide) in Columnar Polyether-Based Discotic Liquid Crystal on the Ionic Conductivity and Dynamics of Lithium Ions

Jih-Dar Hwang, Po-Ying Chen, Shang-Wu Ding * and Chi Wi Ong *

Department of Chemistry, National Sun Yat Sen University, Kaohsiung 804, Taiwan; d022020001@gmail.com (J.-D.H.); silvester032107@gmail.com (P.-Y.C.)

* Correspondence: ding@faculty.nsysu.edu.tw (S.-W.D.); cong@mail.nsysu.edu.tw (C.W.O.)

Received: 11 November 2019; Accepted: 26 November 2019; Published: 28 November 2019

Abstract: The ionic conductivity of an electrolyte is represented by a product of carrier density, charge (electric), and ionic mobility. The overall goal of this study was to provide an insight into the influence of lithium ion conductivity and dynamic when a continuous discotic liquid crystal (DLC) matrix of hexaazatrinapthylene-polyether, HATN-TEG-1, is doped with a small amount of polyethylene oxide (PEO, 5% of MW 8000). The favorable non-covalent interactions between PEO and the DLC triethylene glycol side-chains is supported by the maintenance of the mesophase. The lithium ionic conductivity of HATN-TEG-1 was found to be 1.1×10^{-6} S cm^{-1}, which is better than the corresponding HATN-TEG-1-5%PEO-8000 with a value of 6.06×10^{-7} S cm^{-1}. These results are further supported by the dynamics of the lithium ions in HATN-TEG-1 and HATN-TEG-1-5%PEO-8000 as characterized by ^{7}Li, and ^{1}H NMR spin-lattice relaxation time and self-diffusion coefficient measurements. Though the additional PEO was found to increase the ion carriers, the significant lowering of the ionic conductivity may be attributed to the more pronounced decrease of the mobility of the ionic part when the HATN-TEG-1 matrix is dispersed with PEO. This finding indicates that the doping of 5% PEO onto the matrix of HATN-TEG-1 DLC has an adverse effect on both its diffusion rate and ion conductivity.

Keywords: discotic liquid crystal; polyethylene oxide dispersion; Ionic conductivity; mobility and diffusion coefficients; solid-state ^{1}H and ^{7}Li NMR

1. Introduction

Solid electrolytes with high ionic conductivity are crucial for Li-ion battery performance and have received considerable attention due to the safety considerations arising from the demand for the replacement of liquid electrolytes that are prone to the formation of lithium dendrites that can cause short circuiting and overheating [1,2]. As such, many current liquid electrolytes use a separator in an attempt to alleviate this problem [3]. Though the use of solid electrolytes, especially polymers, may circumvent the restriction of liquid electrolytes, they exhibit low conductivity through the loss of segmental chain motions required for ion-transport upon cooling below the glass transition temperature. Thus, a lithium-polyethylene oxide (PEO) system with an ease of fabrication and low cost has attracted the most attention to date, but it suffers from its low ion conductivity (approximately 10^{-7} S cm^{-1}) at room temperature. Hence, for improving Li-ion conductivity, blended polyethylene oxide-based polymer electrolytes with the addition of liquid electrolytes, plasticizers or inorganic fillers have been designed out to lower the *Tg* and increase the void volume [4].

An alternative method to improve the ionic conductivity is to find anisotropic materials that can provide one directional channel for enhancing ionic conduction. The structural characteristics of liquid crystals (LCs) to form dynamic and order states similar to crystal while retaining some fluidity like an isotropic liquid have been envisaged as good candidates for the next generation of solid electrolytes. LCs bearing a side chain capable of chelating ions upon self-assembly can form one- or two-dimensional ion-conducting pathways and employed as an electrolyte in lithium-ion batteries [5–10], The mesogenic units of the liquid crystals confer the orientational order, whereby the flexible side chains provide complexation with the cations. The liquid-crystalline materials have an added advantage of introducing the possibility of aligning the samples under a magnetic field through the diamagnetism of the mesogenic cores. The most studied liquid crystal electrolytes are the mesogenic cores bearing propylene-carbonate [11,12] and polyether side chains [13,14]. The use of LC derivatives as solid electrolytes cannot be considered as a cost-effective replacement for liquid electrolytes. On the other hand, while polymer electrolytes, such as polyethylene glycol, are cheap, they show poor ion-conductivity. Hence, it would be of great advantages if the introduction of LCs into polymer electrolytes could lead to an increase in the ionic conductivity. To date, only few studies of liquid crystals doped with polymers (PEO or PVA) and cations with the retention of mesogenic properties have been reported. Recently, the addition of 4-cyano-4-pentylbiphenyl, a nematic liquid crystal, to polyvinyl alcohol and potassium iodide was shown to increase ion conductivity, but the liquid crystals were homogeneously dispersed within a polymer matrix in the form of microdroplets rather than forming mesogenic phase. This was due to the phase segregation between the hydrophobic LC and the hydrophilic polymer [15].

Noncovalent orthogonal supramolecular materials have been designed to achieve dynamically functional anisotropic materials [6,16–18]. Recently, the dispersion of various nanoparticles such as metallic, semiconducting and carbon nanostructures into a discotic liquid crystal (DLC) matrix for improving conductivity have received much attention [19]. Though DLC materials have been widely studied for their application as electrolytes [20], their further influences on the lithium ion transport and mobility with the inclusion of polyether oxide onto the liquid crystalline matrix have not been reported. Liquid crystal polymer blends can be divided into two categories: (1) A small amount of nematic liquid crystalline material (up to 30%) is dispersed in a continuous polymer matrix, and (2) a minute amount of polymer (approximately 5%) is dispersed in a continuous discotic liquid crystalline nanochannels [21,22]. In the present study, we designed a discotic liquid crystal with six-triethylene glycol side chains, HATN-TEG-1, that form a hexagonal columnar liquid-crystalline phase. Herein, we focus on DLC as the continuous matrix, whereby a small amount of PEO (5%) is dispersed into liquid crystalline nanochannels. Our results show a favorable inclusion of 5% PEO-8000 into HATN-TEG-1 with the maintenance of the mesophase. Moreover, the further inclusion of $LiCO_4$ salt for solid electrolyte application did not disrupt the mesophase.

Our main objective in this study was to determine the influence of the inclusion of PEO into the nanochannels of HATN-TEG-1 on the lithium ions' conductivity and mobility, as well as to obtain a better understanding on the diffusion pathway for lithium-ion batteries.

2. Materials and Methods

2.1. Liquid Crystallin Properties

Thermal behavior (mesogenic properties) was investigated using a Perkin Elmer Pyris DSC 4000 differential scanning calorimeter (Perkin Elmer Instrument, Netherland). The phase behavior was studied using a Nikon model ECLIPSE LV100 OPL (Nikon Inc., China) polarizing light microscope equipped with a Linkam LTS420E-P hot stage (Linkam Scientigic Instument, United Kingdom). X-Ray diffraction data were collected on the wiggler beamline BL17A at the National Synchrotron Radiation Research Center (NSRRC), Taiwan, by using a triangular bent Si (111) monochromator at a wavelength of 1.320898 A° with the sample in a 1 mm capillary tube (WJM-Glas/Muller GmbH).

Nuclear magnetic resonance spectra were recorded on a JEOL ECZ600R(600MHz) (Joel Inc, Japan) spectrometer. Chemical shifts are reported in ppm relative to residual $CHCl_3$ δ 7.26, ^{1}H; δ 77.00, ^{13}C). Mass spectra were obtained on Bruker Daltonics, autoflex III TOF/TOF (Bruker GmbhCity, Germanuy). (See Supplementary Materials)

Electrolyte complexes were formed by using percentage weight amounts of HATN-TEG-1 and PEO-8000, together with a fixed amount of $LiClO_4$ (1 equivalent based on HATN-TEG-1). The electrolytes were prepared by stirring in HPLC grade ethanol until homogenous at room temperature. The solvent was removed by using a rotatory evaporator under vacuo, and the resultant mixture was dried under high vacuum for 5 h at room temperature.

2.2. Conductivity Measurement

The conductivity of the samples was measured on a Metrohm Autolab BV (The Netherlands). The sample was placed between two ITO electrodes and sealed with AB epoxy glue to ensure close contact between the sample and the electrodes (Figure 1). The conductivity of each sample could be calculated from the resistance from the Nyquist plot displayed on the instrument.

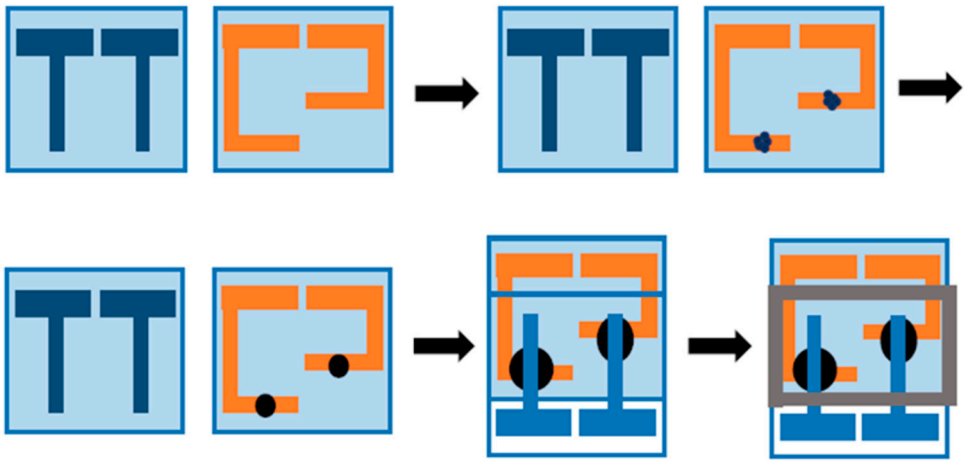

Figure 1. Assemble of the cell for conductivity measurements.

Cell gap measurement and impedance:

$$\sigma = L/\Omega * A \quad (1)$$

whereby σ is the conductivity, L is the cell gap, A is the overlap area, and Ω is resistance in equation (1) obtained by the Nyquist plot.

2.3. NMR Spectroscopy and Diffusion

The measurement of NMR spectra relaxation rate and diffusion coefficient were performed on a Varian Inova 500 MHz solid state NMR spectrometer equipped with a micro-imaging unit. Experiments were carried out without sample spinning. The ^{1}H and ^{7}Li spectra were obtained with single pulse excitation. An inversion recovery pulse sequence was employed for T_1 (longitudinal relaxation time) measurements and CPMG spin echo sequence was employed for T_2 (transverse relaxation time) measurements. The T_1 values were obtained by fitting the experimental data with exponential growth function $M(\tau) = M_0\ (1-2\varepsilon^{-\tau/T}{}_1)$, where τ is the length of longitudinal relaxation period. The T_2 values were obtained by fitting the experimental data with exponential decay function $M(\tau) = M_0\ \varepsilon^{-\tau/T}{}_2)$, where τ is the length of transverse relaxation period.

The self-diffusion coefficient of ^{7}Li was measured with the pulse gradient field (PFG) method. The spin echo pulse sequence was used. The pulse gradient field used was varied between −60 and 60 G/cm with a width of 2 s. The signal was fitted according to an exponential decay function, $M(\tau)$

$= M_0\ e^{ag^2D}$), where D is diffusion coefficient, g is the variable gradient field, e and a is a variable depending on the strength and width of the pulse gradient fields and the intervals between pulses.

All experiments were carried out at room temperature of 25 °C

2.4. Synthesis

The 1,2-diamino-4,5-bis(2-(2-methoxyethoxy)ethoxy)ethoxybenzene was synthesized according to published procedure [23,24].

The hexa-triethylene glycol-hexaazatrinapthylene (HATN-TEG-1) was prepared by the condensation of 1,2-diamino-4,5-bis(2-(2-methoxyethoxy)ethoxy)ethoxybenzene (7.78 g, 18.0 mM)) with hexaketocyclohexane octahydrate (1.50 g; 4.8 mM) in refluxing ethanol (30 mL) and acetic acid (30 mL) under nitrogen for 24 h. The solvents were then removed using a rotatory evaporator under vacuo. The residue was dissolved in dichloromethane and washed with $NaHCO_3$ (aq) and brine, dried over anhydrous $MgSO_4$, filtered through a pad of Celite, and concentrated in vacuo. The residue was rigorously purified by column chromatography using silica gel (eluent: dichloromethane/methanol = 20/1). ^{1}H-NMR(300 MHz, $CDCl_3$): orange gum (38% yield); δ 7.85 (s, 6H), 4.44 (t, 12H, J = 4.5 Hz), 4.06 (t, 12H, J = 4.5 Hz), 3.84 (t, 12H, J = 4.5 Hz), 3.57 (t, 12H, J = 4.5 Hz), 3.74~3.67 (m, 24H), and 3.38 (s, 18H); ^{13}C NMR (CDCl3, 125 MHz) d 154.2 (Ar–C), 141.2 (Ar–C), 140.7 (Ar–H), 107.7 (Ar-C), 71.9.(Ar-O-CH_2), 71.0 (-OCH_2CH_2O-), 70.7 (-OCH2CH2O-), 70.5 (-OCH_2CH_2O-), 69.1 (-OCH_2CH_2O-), 69.0 (-OCH_2CH_2O-), 59.0 (-OCH_3); MS *m/z* HRMS (ESI) calculated for $C_{66}H_{96}N_6O_{24}$ (M+H) 1357.65566, found: 1357.6541.

3. Results and Discussion

3.1. Synthesis and Liquid Crystalline Properties

The synthesis of 2,3,8,9,14,15-hexa(2-(2-methoxyethoxy)ethoxy)ethoxy-diquinoxalino[2,3-*a*:2¢,3¢-*c*]phenazine (HATN-TEG-1) was accomplished by using our modified approach through the direct condensation of hexaketocyclohexane with 1,2-bisalkoxy-4,5-diaminobenzene (Scheme 1) [25]. It is noteworthy to point out that the metal promoted oxidative trimerization of I,2-bis(2-(2-methoxy-ethoxy)ethoxy)ethoxybenzene could not be used to prepare the triphenylene derivatives. Similarly, the Friedel–Crafts reaction between I,2-bis(2-(2-methoxy-ethoxy)ethoxy)ethoxybenzene and oxalyl chloride could not be successfully carried out to give 2,3,6,7-tetra(2-(2-methoxyethoxy)-ethoxy)ethoxy-phenanthrene-9,10-diones. We attribute this to the strong coordination of the polyether side chains with the metal ions of the reagents required for the reaction.

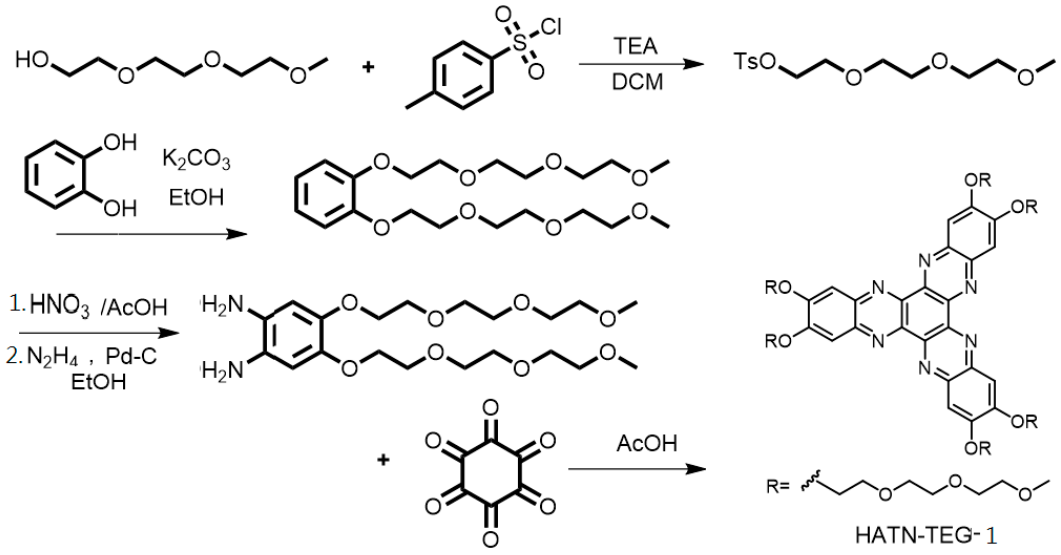

Scheme 1. Synthetic scheme of HATN-TEG-1.

The mesogenic properties of HATN-TEG-1 and HATN-TEG-1– 5% PEO-8000 were investigated by using polarized optical microscopy (POM), differential scanning calorimetry (DSC), and variable temperature X-ray diffraction (XRD). The POM studies showed that all the samples mentioned above exhibited liquid crystalline properties upon cooling from an isotropic temperature (Figure 2). Interestingly, HATN-TEG-1 and HATN-TEG-1–5% PEO-8000 retained the birefringent texture on further cooling to room temperature (Figure 2). The DSC measurement of HATN-TEG-1 and HATN-TEG-1–5% PEO-8000 from −20 to 220 °C did not show any endothermic peaks during the second and third cooling cycle, revealing room temperature liquid crystalline properties. This is in accordance with the reported properties of polyether side chains containing liquid crystals which are intrinsically resistant to crystallization due to their inability to efficiently pack, together with the lowering of mesogenic temperatures which is of great importance for their application as electrolytes [26]. The XRD diffraction peaks observed for HATN-TEG-1 and HATH-TEG-1-5%PEO-8000 in Table 1 showed one very sharp strong reflection indexed as (100) and the second weak reflection indexed as (110) with a reciprocal spacing ratio of 1:($\sqrt{3}$) for a Col_h lattice at room temperature at the small angle region. In the case of HATN-TEG-1, a disc–disc intramolecular distance was shown to be around 3.44 Å and a calculated lattice constant of 27.28 Å. Interestingly, the mixing of 5% PEO-8000 with HATN-TEG-1 did not cause any significant expansion or disruption to the columnar hexagonal arrangement, whereby the disc–disc intramolecular distance remained around 3.48 A ° with a calculated lattice constant of 27.96 Å. This value for HATH-TEG-1-5%PEO-8000 was only slightly larger than that observed for HATN-TEG 1. This is similar to the numerous signals with the intraplanar spacings corresponding to the indexation (hkl) according to the report of side-chain liquid crystalline polyethers and polyamines polymer with columnar liquid crystal assembly with proton and ionic channels by Giamberini et al. [27–30]. These observations indicate the efficient accommodation of 5% PEO-8000 into the hexagonal columnar matrix of HATN-TEG-1. Moreover, the additional diffraction indexed at (200) and (210) for HATN-TEG-1 clearly indicate a more ordered assembly as compared to that of HATH-TEG-1-5%PEO.

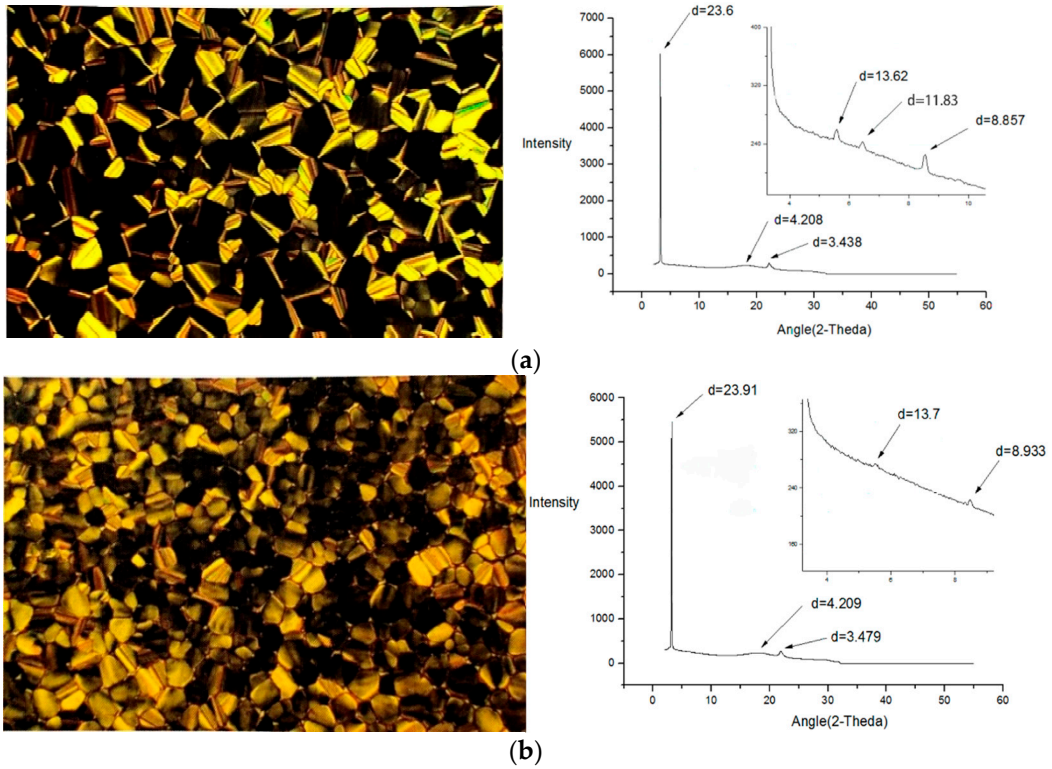

Figure 2. The polarized optical microscopy (POM) texture and powder X-ray diffraction patter of (**a**) HATN-TEG-1 and (**b**) HATN-TEG-1-5% polyethylene oxide (PEO)-8000.

Table 1. XRD data of HATN-TEG-1 during cooling from isotropic to room temperature (λ = 1.320898 Å).

Compound	Angle (2θ)	d_{obs} (Å)	d_{cal}(Å)	Miller Index (h,k,l)	Lattice Constant (Å)
HATN-TEG-1	3.2073	23.600	23.60	(100)	27.25
	5.5588	13.620	13.63	(110)	
	6.40078	11.830	11.80	(200)	
	8.55281	8.857	8.92	(210)	
	18.0559	4.208		halo	
	22.151	3.438		core to core	
HATN-TEG-1 -5%PEO-MW8000	3.1657	23.910	23.91	(100)	27.61
	5.52637	13.700	13.80	(110)	
	8.47991	8.933	9.04	(200)	
	18.0556	4.209		halo	
	21.8868	3.479		core to core	
HATN-TEG-1 –$LiClO_4$	3.0683	24.699	24.67	(100)	28.49
	5.15472	14.687	14.24	(110)	
	22.5835	3.373		core to core	
HATN-TEG-1 -5%PEO-MW8000–$LiClO_4$	3.13734	24.126	24.13	(100)	27.86
	22.2487	3.433		core to core	

The POM and XRD experimental results (Figure 3) indicate that $LiClO_4$ dispersed in the HATN-TEG-1 and HATH-TEG-1-5%PEO-8000 columnar matrix without disrupting the mesophase. The HATH-TEG-1-5%PEO-8000–$LiClO_4$ showed large domains of dendritic growth as the sample was slowly cooled to room temperature. The XRD patterns of these composites show similar intercolumnar distances as compared to the starting compounds, indicating the inclusion of $LiClO_4$ to the columnar matrix did not destabilize the self-assembly and retained the mesophase structure. These composites did not show prominent peak during the second and third heating and cooling cycle in the DSC thermogram. The XRD profile of HATN-TEG-1–$LiClO_4$ showed only two diffraction peaks indexed as (100) and (110) with a reciprocal spacing ratio of 1:($\sqrt{3}$) for a Col_h and lattice constant of a 28.49 Å (Table 1); they were thus less ordered. The presence of PEO and $LiClO_4$ in the HATN-TEG-1 nanochannels made the assembly become more disordered, and we could only observe the diffraction peak indexed at (100).

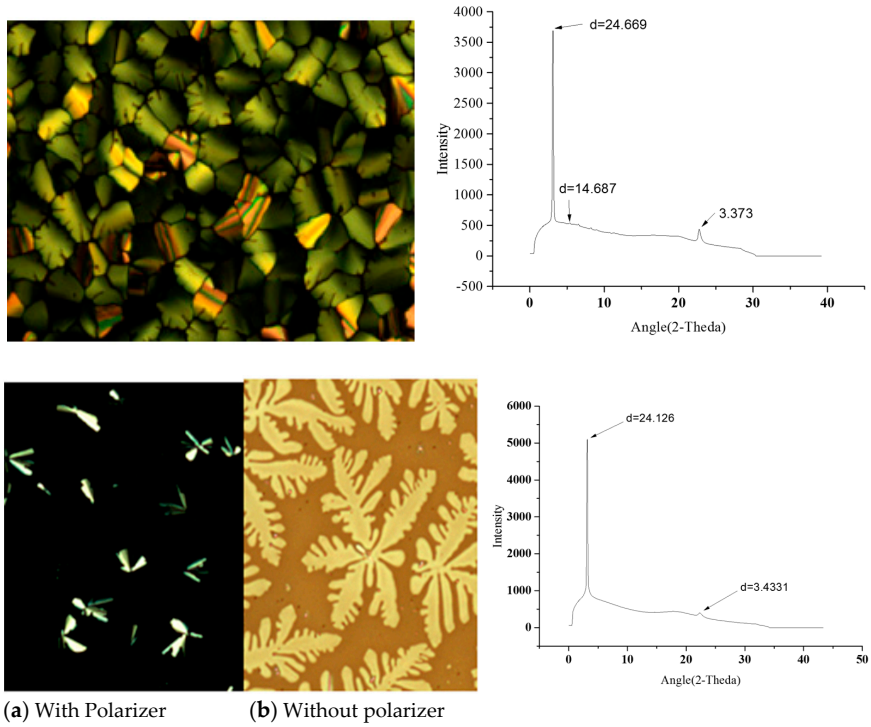

(**a**) With Polarizer (**b**) Without polarizer

Figure 3. The POM texture and powder X-ray diffraction pattern of (**a**) HATN-TEG-1–$LiClO_4$ and (**b**) HATN-TEG-1-5% PEO-8000–$LiClO_4$.

3.2. Ion Conductivity

The conducting behavior of HATN-TEG-1–$LiClO_4$ and HATN-TEG-1–5% PEO-8000–$LiClO_4$ can be clearly seen in the impedance plot of Z″ against Z′ (Figure 4). The samples were heated to isotropic point under POM and allowed to cool to room temperature. The HATN-TEG-1–$LiClO_4$ showed a conductivity of 1.1×10^{-6} S/cm. Surprisingly, HATN-TEG-1–5% PEO-8000–$LiClO_4$ had a much lower conductivity of 6.06×10^{-7} S/cm; nearly an order of decrease in conductivity as compare to HATN-TEG–$LiClO_4$. Our observed results show that the dispersion of 5% PEO onto the polyether matrix of HATN-TEG-1 DLC failed to improve the ionic conductivity. It is known that ionic conductivity is the modulation of carrier density, charge (electric), and ionic mobility. Accordingly, the HATN-TEG-1 side chain with the doping of PEO onto the nanochannels can have a higher polarity for dissociating ions. In contrast, PEO in the DLC-polyether nanochannels can also have a counteracting effect by decreasing the flexibility and increasing the viscosity of the polyether conducting regions, thus adversely lowering ionic mobility.

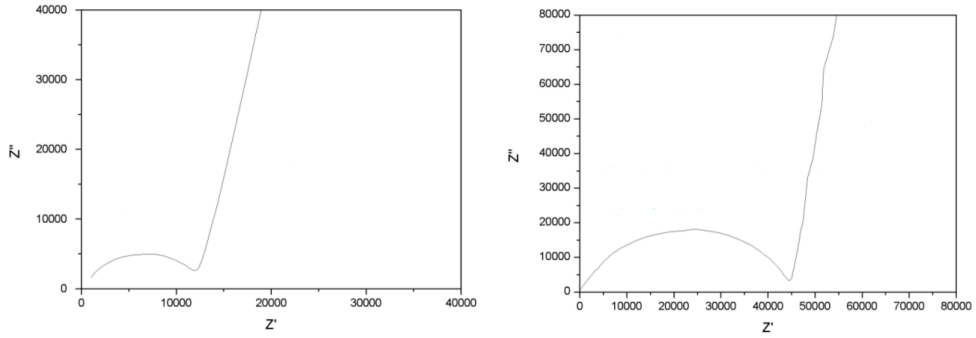

Figure 4. The Nyquist plot of (**a**) HATN-TEG-1 + 1 .0 equivalence $LiClO_4$ and (**b**) HATN-TEG-1 + 5 wt%PEO MW 8000 + 1.0 equivalence $LiClO_4$.

3.3. Mobility and Self-Diffusion Coefficients of Lithium Ions

The studies on the influence of structural order or disorder on the diffusion of mobile lithium ions using ^{7}Li NMR were carried out for HATN-TEG-1 and HATN-TEG-1-5% PEO-8000 at glass transition state at room temperature. The ^{1}H and ^{7}Li spectra of HATN-TEG-1–$LiClO_4$ and HATN-TEG-1-5% PEO-8000–$LiClO_4$ are shown in Figure 5. The spectra widths of ^{1}H spectra were 6.0 and 7.0 ppm (300 and 350 Hz) for HATN-TEG-1–$LiClO_4$ and HATN-TEG-1-5%-PEO-8000–$LiClO_4$, respectively. Compared to the 100 kHz ^{1}H NMR spectral width of a typical solid organic compound, these spectral widths were very narrow. This means these samples were highly dynamic, consistent with the fact that they are liquid crystals, which was confirmed by the narrow ^{7}Li spectra of these samples (6.0 and 7.5 ppm, respectively). It is worth noting that the spectral width of HATN-TEG-1–$LiClO_4$ (both ^{1}H and ^{7}Li spectra) was only slightly narrower than that of HATN-TEG-1-5% PEO-8000–$LiClO_4$, indicating that the internal motion of pure HATN-TEG-1 was slightly faster than that when dispersed with 5% PEO. Though the line-width corresponds to a rotational diffusion of the molecules, this fact is an indication of the lithium ions diffusion rate in these samples.

The ^{7}Li longitudinal relaxation times of the samples could be calculated by fitting the evolution of the spectral profiles given in Figure 6. The transverse relaxation times by fitting the NMR spectra at different echo times are shown in Figure 7. The T_1 and T_2 values are given in Table 2. It was found that HATN-TEG-1–$LiClO_4$ had shorter T_1 and T_2 values than HATN-TEG-1-5%-PEO-8000–$LiClO_4$. The translational diffusion coefficient of lithium cation could be obtained by fitting the spectral profile similar to that shown in Figure 7 by inputting the lengths and intensities of the gradient field pulses used in the PFG experiment. The results are summarized in Table 2. It is clear that HATN-TEG-1–$LiClO_4$ had a faster translational diffusion. Therefore, there was a positive correlation between the rotational diffusion rate (measured from nuclear relaxation) and translational diffusion rate in these samples.

This could be understood because in these samples the fluctuation of magnetic field on the ^{7}Li nuclei, which is responsible for nuclear relaxation, was indeed primarily caused by the translational motion of the lithium cations.

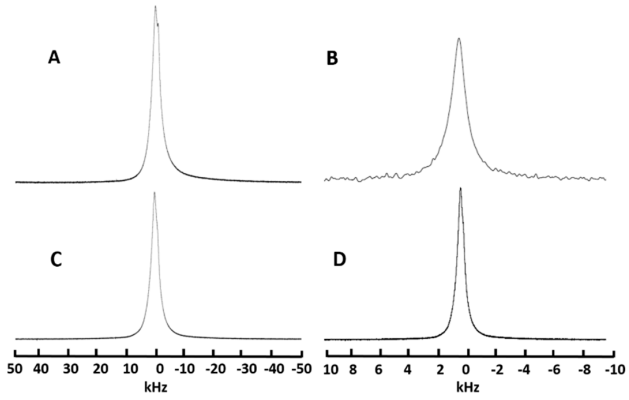

Figure 5. (i) HATN-TEG-1–$LiClO_4$ static ^{1}H (**A**) and ^{7}Li (**B**) NMR spectra; (ii) HATN-TEG-1–5% PEO-8000–$LiClO_4$. static ^{1}H (**C**) and ^{7}Li (**D**) NMR spectra.

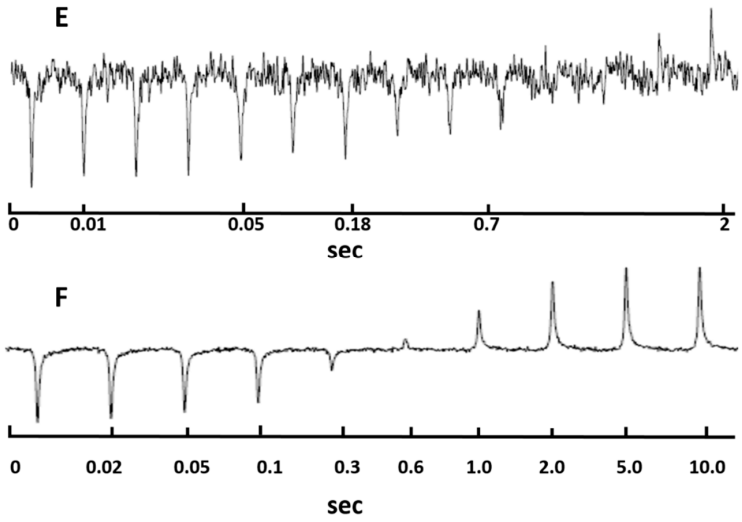

Figure 6. The inversion-recovery profiles of ^{7}Li longitudinal relaxation. (**E**) for HATN-TEG-1–$LiClO_4$ and (**F**) for HATN-TEG-1-5% PEO–$LiClO_4$.

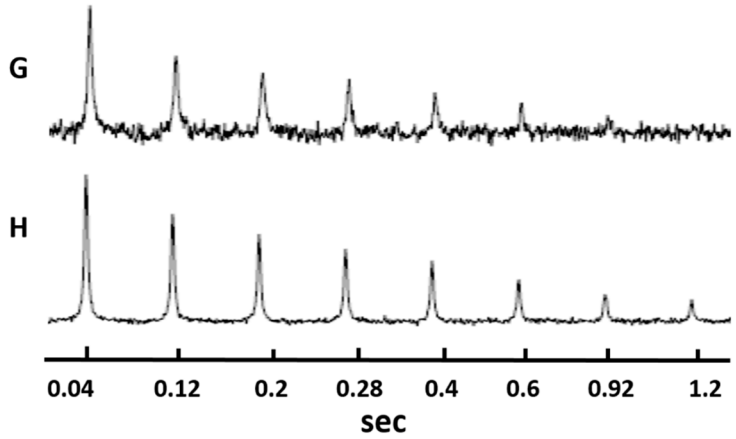

Figure 7. The ^{7}Li self-diffusion/T_2 (transverse relaxation time) spectral profiles. (**G**) for HATN-TEG-1–$LiClO_4$ and (**H**) for HATN-TEG-1-5% PEO–$LiClO_4$.

Table 2. The longitudinal relaxation time (T_1), transverse relaxation time (T_2) and translational diffusion coefficient (D) of ^{7}Li in three different samples, as compared to their conductivity (σ).

Sample	T_1(s)	T_2(ms)	D(10^{-9} cm^2/s)	σ(10^{-7} S/cm)
HATN-TEG-1–$LiClO_4$	0.72 +/−0.05	0.8 +/−0.1	2.11 +/−0.05	11.0 +/−0.1
HATN-TEG-1-5% PEO–$LiClO_4$	1.15 +/−0.1	1.6 +/−0.1	1.16 +/−0.03	6.06 +/−0.05

Note: These values are the average of many liquid crystals orientated in many different directions because the samples were not prepared in a single orientation.

By comparing the translational diffusion rate and conductivity, a fairly good positive correlation can be seen in Table 2. Because conductivity is proportional to the product of the charge density and diffusion rate, this correlation means that the concentrations of lithium cations were almost the same in the two samples, as the difference in conductivity was caused by the mobility of lithium cations moving faster in HATN-TEG-1–$LiClO_4$.

This was consistent with the compositions of the two samples in which the same percentage of $LiClO_4$ was used (ignoring the 5% w/w PEO used). The role of PEO on diffusion rate and conductivity was intriguing—when a small percentage (5%) of PEO was added, both the diffusion and conductivity dropped compared with pure HATN-TEG-1. This suggests that when a small amount of PEO is added, it blocks or distorts the pathways of lithium ions in a HATN-TEG-1 matrix.

These results demonstrate that NMR studies of Li and ^{1}H relaxation rates and diffusion can provide valuable information about the structure and dynamics relevant to the ionic conductivity in materials. In particular, the good agreement between translational diffusion coefficient and conductivity enables us to pin down the microscopic mechanism of ion conduction. In this case, for example, we have clear evidence that the ion density (carrier density) was largely the same in the two samples; the difference between conductivity was caused by different diffusion rates.

4. Conclusions

In conclusion, 5% PEO can be well accommodated within the matrix of HATN-PEG-1 that bears a columnar hexagonal architecture. Furthermore, we have painted a clearer picture of the lithium ion conductivity and dynamics of HATN-PEG-1 and after 5% PEO is dispersed into the matrix of HATN-TEG-1-5% PEO. The present results indicate that, although the dispersion of 5% PEO into HATN-PEG-1 can favorably increase ion carriers, this is overridden by the unfavorable chain segmental motions which retard ions diffusion, as shown by the NMR and ionic conductivity studies

Supplementary Materials: The following are available online at http://www.mdpi.com/2073-4352/9/12/627/s1, Figure S1: ^{1}H NMR and ^{13}C NMR of HATN-TEG-1, DSC second and third run of HATN-TEG-1, HATN-TEG-1: 1.0 equiv. $LiClO_4$, HATN-TEG-1-5%PEO and HATN-TEG-1-5%PEO: 1.0 equiv. $LiClO_4$

Author Contributions: J.-D.H.; methodology, validation, writing—review and editing, P.-Y.C.; investigation and data curation, S.-W.D.; NMR diffusion studies and formal analysis, and C.W.O.; writing—original draft preparation, supervision, and funding acquisition.

Funding: We acknowledge the generous financial support by the Ministry of Science and Technology, and National Synchrotron Radiation Center, Taiwan for the research and studentship award.

Acknowledgments: We thank the National Synchrotron Radiation Center, Taiwan for performing the variable temperature XRD experiments.

Conflicts of Interest: The authors declare there is no conflict of interest in this research for publication.

References

1. Mayers, M.; Kaminski, J.; Miller, T. Suppression of dendrite formation via pulse charging in rechargeable lithium metal batteries. *J. Phys. Chem. C* **2012**, *116*, 26214–26221. [CrossRef]
2. Seong, I.W.; Hong, C.H.; Kim, B.K.; Yoon, W.Y. The effects of current density and amount of discharge on dendrite formation in the lithium powder anode electrode. *J. Power Sources* **2008**, *178*, 769–773. [CrossRef]

3. Lee, H.; Yanilmaz, M.; Toprakci, O.; Fu, K.; Zhang, X. A review of recent developments in membrane separators for rechargeable lithium-ion batteries. *Energy Environ. Sci.* **2014**, *7*, 3857–3886. [CrossRef]
4. Funahashi, M.; Shimura, H.; Yoshio, M.; Kato, T. Functional liquid-crystalline polymers for ionic and electronic conduction. *Struct. Bond.* **2008**, *128*, 151–179.
5. Demus, D.; Goodby, J.; Gray, G.W.; Spiess, H.-W.; Vill, V. (Eds.) *Handbook of Liquid Crystals*; Wiley-VCH: Weinheim, Germany, 1998; Volume 2A, Low Molecular Weight Liquid Cristals I.
6. Kato, T.; Mizoshita, N.; Kishimoto, K. Functional liquid-crystalline assemblies: Self-organized soft materials. *Angewandte Chemie Int. Ed.* **2006**, *45*, 38–68. [CrossRef]
7. Sergeyev, S.; Pisula, W.; Geerts, Y.H. Synthesis and properties of macrodiscotic triphenyleno-phthalocyanines. *Chem. Soc. Rev.* **2007**, *36*, 1902–1929. [CrossRef]
8. Gin, D.L.; Lu, X.; Nemade, P.R.; Pecinovsky, C.S.; Xu, Y.; Zhou, M. Recent advances in the design of polymerizable lyotropic liquid crystal assemblies for heterogeneous catalysis and selective separations. *Adv. Funct. Mater.* **2006**, *16*, 865–878. [CrossRef]
9. Ikeda, T.; Mamiya, J.; Yu, Y.L. Photomechanics of liquid-crystalline elastomers and other polymers. *Angewandte Chemie Int. Ed.* **2007**, *46*, 506–528. [CrossRef]
10. Högberg, D.; Soberats, B.; Uchida, S.; Yoshio, M.; Kloo, L.; Segawa, H.; Kato, T. Nanostructured two-component liquid-crystalline electrolytes for high-temperature dye-sensitized solar. *Chem. Mater.* **2014**, *26*, 6496–6502. [CrossRef]
11. Sakuda, J.; Hosono, E.; Yoshio, M.; Ichikawa, T.; Matsumoto, T.; Ohno, H.; Zhou, H.; Kato, T. Liquid-crystalline electrolytes for lithium-ion batteries: Ordered assemblies of a mesogen-containing carbonate and a lithium salt. *Adv. Funct. Mater.* **2015**, *25*, 1206–1212. [CrossRef]
12. Kerr, R.L.; Edwards, J.P.; Jones, S.C.; Elliott, B.J.; Gin, D.L. Effect of varying the composition and nanostructure of organic carbonate-containing lyotropic liquid crystal polymer electrolytes on their ionic conductivity. *Polym. J.* **2016**, *48*, 635–643. [CrossRef]
13. Ohtake, T.; Takamitsu, Y.; Ito-Akita, K.; Kanie, K.; Yoshizawa, M.; Mukai, T.; Ohno, H.; Kato, T. Liquid-crystalline ion-conductive materials: Self-organization behavior and ion-transporting properties of mesogenic dimers containing oxyethylene moieties complexed with metal salts. *Macromolecules* **2000**, *33*, 8109–8111. [CrossRef]
14. Stoeva, Z.; Lu, Z.; Ingram, M.D.; Imrie, C.T. A new polymer electrolyte based on a discotic liquid crystal triblock copolymer. *Electrochimica Acta* **2013**, *93*, 279–286. [CrossRef]
15. Said, S.M.; Zulkifli, A.Z.S.; Kamarudin, M.A.; Mainal, A.; Subramanian, B.; Mohamed, N.S. Polymer electrolyte liquid crystal system for improved optical and electrical properties. *Eur. Polym. J.* **2015**, *66*, 266–272. [CrossRef]
16. Brunsveld, L.; Folmer, B.J.B.; Meijer, E.W.; Sijbesma, R.P. Supramolecular polymers. *Chem. Rev.* **2001**, *101*, 4071–4097. [CrossRef]
17. Elacqua, E.; Lye, D.S.; Weck, M. Engineering orthogonality in supramolecular polymers: From simple scaffolds to complex materials. *Acc. Chem. Res.* **2014**, *47*, 2405–2416. [CrossRef]
18. Kato, T.; Uchida, I.; Ichikawa, T.; Sakamoto, T. Functional liquid crystals towards the next generation of materials. *Angewandte Chemie Int. Ed.* **2018**, *57*, 4355–4371. [CrossRef]
19. Gowda, A.; Kumar, S. Recent advances in discotic liquid crystal-assisted nanoparticles. *Materials* **2018**, *11*, 382. [CrossRef]
20. Kato, T.; Yoshio, M.; Ichikawa, T.; Soberats, B.; Ohno, H.; Funahash, M. Transport of ions and electrons in nanostructured liquid crystals. *Nat. Rev. Mat.* **2017**, *2*, 17001. [CrossRef]
21. Jákli, A. Structure and optical properties of liquid crystal dispersed polymers. *Mol. Cryst. Liq. Cryst.* **1994**, *251*, 289–301. [CrossRef]
22. Dierking, I. Polymer, network-stabilized liquid crystals. *Adv. Mater.* **2000**, *12*, 167–181. [CrossRef]
23. Ouchi, M.; Inoue, Y.; Liu, Y.; Nagamune, S.; Nakamura, S.; Wada, K.; Hakushi, T. Convenient and efficient tosylation of oligoethylene glycols and the related alcohols in tetrahydrofuran-water in the presence of sodium hydroxide. *Bull. Chem. Soc. Jpn.* **1990**, *63*, 1260–1262. [CrossRef]
24. Yeh, M.C.; Liao, S.C.; Chao, H.; Ong, C.W. Synthesis of polyphilic hexaazatrinaphthylenes and mesomorphic properties. *Tetrahedron* **2010**, *66*, 8888–8892. [CrossRef]

25. Ong, C.W.; Liao, S.-C.; Chang, T.H.; Hsu, H-F. In situ synthesis of Hexakis(alkoxy)diquinoxalino [2,3-a:2′,3′-c]phenazines: Mesogenic phase transition of the electron-deficient discotic compounds. *J. Org. Chem.* **2004**, *69*, 3181–3185. [CrossRef]
26. Stowe, M.K.; Liu, P.; Baker, G.L. Star poly(ethylene oxide) as a low temperature electrolyte and crystallization inhibitor. *Chem. Mater.* **2005**, *17*, 6555–6559. [CrossRef]
27. Bogdanowicz, K.A.; Pirone, D.; Prats-Reig, J.; Ambrogi, V.; Reina, J.A.; Giamberini, M. In situ raman spectroscopy as a tool for structural insight into cation non-ionomeric polymer interactions during ion transport. *Polymers* **2018**, *10*, 416. [CrossRef]
28. Bogdanowicz, K.A.; Bhosale, S.V.; Li, Y.; Vankelecom, F.J.; Garcia-Valls, R.; Reina, J.A.; Giamberini, M. Mimicking nature: Biomimetic ionic channels. *J. Membr. Sci.* **2016**, *509*, 10–18. [CrossRef]
29. Montane, X.; Bogdanowicz, K.A.; Colace, G.; Reina, J.A.; Cerruti, P.; Lederer, A.; Giamberini, M. Advances in the design of self-supported ion-conducting membranes new family of columnar liquid crystalline polyamines. Part 1: Copolymer synthesis and membrane preparation. *Polymer* **2016**, *105*, 298–309. [CrossRef]
30. Bogdanowicz, K.A.; Rapsilber, G.A.; Reina, J.A.; Giamberini, M. Liquid crystalline polymeric wires for selective proton transport, part 1: Wires preparation. *Polymer* **2016**, *92*, 50–57. [CrossRef]